
Theses and Dissertations

Spring 2017

Development of compact collimation device for novel scanning beam low-energy intraoperative radiation therapy (SBIORT) system for pancreatic cancer

Brennen Neal Wears
University of Iowa

Follow this and additional works at: <https://ir.uiowa.edu/etd>



Part of the [Mechanical Engineering Commons](#)

Copyright © 2017 Brennen Neal Wears

This thesis is available at Iowa Research Online: <https://ir.uiowa.edu/etd/5678>

Recommended Citation

Wears, Brennen Neal. "Development of compact collimation device for novel scanning beam low-energy intraoperative radiation therapy (SBIORT) system for pancreatic cancer." MS (Master of Science) thesis, University of Iowa, 2017.

<https://doi.org/10.17077/etd.te9lx7r0>

Follow this and additional works at: <https://ir.uiowa.edu/etd>



Part of the [Mechanical Engineering Commons](#)

Development of Compact Collimation Device for Novel Scanning Beam Low-Energy Intraoperative Radiation Therapy (SBIORT) System for Pancreatic Cancer

by

Brennen Neal Wears

A thesis submitted in partial fulfillment
of the requirements for the Master of Science
degree in Mechanical Engineering in the
Graduate College of
The University of Iowa

May 2017

Thesis Supervisor: Associate Professor Junyi Xia

Copyright by
BRENNEN NEAL WEARS
2017
All Rights Reserved

Graduate College
The University of Iowa
Iowa City, Iowa

CERTIFICATE OF APPROVAL

MASTER'S THESIS

This is to certify that the Master's thesis of

Brennen Neal Wears

has been approved by the Examining Committee for
the thesis requirement for the Master of Science degree
in Mechanical Engineering at the May 2017 graduation.

Thesis Committee:

Junyi Xia, Thesis Supervisor

Albert Ratner

Hiroyuki Sugiyama

Acknowledgements

I would first like to thank my research adviser Junyi Xia. Thank you Junyi, for your guidance and support through both my undergraduate and graduate research. I would also like to thank my academic adviser Albert Ratner for his guidance through my graduate education and Hiroyuki Sugiyama for his willingness to serve on my thesis committee. I would like to acknowledge the work and support of Ryan Flynn, Imran Mohiuddin, Yusung Kim, Timothy Woldron, and Bryan Allen who have all made contributions to the development of this project.

Abstract

Intraoperative radiation therapy (IORT) involves delivering high doses of radiation directly to tumors while sparing healthy tissues in a surgical setting. Current IORT systems lack the capability to deliver conformal radiation therapy. To overcome the limitations of non-conformal radiation therapy a collimation system is needed to conform the radiation beam to the shape of the tumor. This work presents the development of a compact collimator design intended for a scanning beam IORT (SBIORT) system. The SBIORT collimator design enables the delivery of variable square doses to the targeted region within the surgical cavity. The SBIORT collimator has a compact circular footprint of 66 mm diameter and 10 mm thickness, with a maximum aperture of 20 mm. SBIORT collimator was prototyped to validate the design in positional accuracy and dosimetry experiments. Accuracy of the collimator leaf position was ± 0.25 mm at a 95% confidence interval. Dosimetric evaluation revealed the collimator to have a penumbra of 1.9 mm with a leaf transmission of 0.5%. The results support the feasibility of implementing the compact SBIORT collimator design in IORT.

Table of Contents

List of Figures	vi
Chapter 1 - Introduction.....	1
1.2 Intraoperative Radiation Therapy.....	2
1.3 Objective for SBIORT	4
1.3.1 SBIORT Project.....	5
1.4 Collimation.....	6
1.4.1 Multi-Leaf Collimator	7
1.4.2 Camera Shutter/Aperture	8
1.5 Organization of the Document	9
Chapter 2 - Design Considerations SBIORT Collimator.....	10
2.1 Design Objectives and Constraints	10
2.2 Multi-Leaf Collimator Design.....	12
2.2.1 Conclusion: Multi-Leaf Collimator Design.....	14
2.3 Iris Diaphragm Shutter	15
2.3.1 Conclusion: Iris Diaphragm Shutter	19
Chapter 3 - SBIORT Collimation Design.....	21
3.1 Dynamics of Collimator Design.....	22
3.2 Optimizing Size.....	23
3.3 Developing Design.....	24
3.3.1 Leaf Design.....	26
3.4 Manufacturing Prototypes	27
Chapter 4 - Experimental Validation	29
4.1 Collimator Position Accuracy Test	29
4.2 Dosimetry Experiment	30
Chapter 5 - Experimental Results	33
5.1 Collimator Positional Results.....	33
5.2 Dosimetry Results	34
Chapter 6 - Discussion and Considerations	37
6.1 Discussion Collimator	37
6.2 Discussion Dosimetry	39

Chapter 7 - Conclusion	41
References.....	44

List of Figures

Figure 1: IORT applicator positioned in the surgical cavity of a patient with pancreatic cancer [20]	4
Figure 2: a) close-up of the of SBIORT system and b) model of SIORT system on mobile cart used to maneuver in surgical rooms. 3D scanning used to model the topography of the surgical cavity to be used in treatment planning process. The six-axis robot arm will maneuver the radiation source and collimator along the optimum path while the collimation system dynamically adjusts itself to effectively irradiate the desired region.....	6
Figure 3: a) Radiation beam collimated with multi-leaf collimator and b) inside view of multi-leaf collimator [25].....	8
Figure 4: a) 2-dimensional pattern generated by a MLC to conform to tumor shape and b) comparison of geometric packing of an arbitrary shape using squares vs circles	11
Figure 5: a) SBIORT MLC linkage design and b) linkage optimization parameters	13
Figure 6: SBIORT MLC linkage optimization	14
Figure 7: Six-blade iris diaphragm cycled from a closed state to open (Stage 1-3) and an isometric view (bottom)	16
Figure 8: Alternative iris shutter design with two counter-rotating discs, a) with a cover, and b) without cover	17
Figure 9: Kinematic analysis of alternative iris shutter design with two counter-rotating discs, a) the kinematic linkages overlaid on the CAD drawings, and b) the linkage system at two separate positions	18
Figure 10: Angular position of the alternative iris blade as it is cycled open.....	19
Figure 11: Patent pending dynamic collimator design, a) with top cover on, and b) without top cover	21
Figure 12: a) Planar four-bar and b) kinematic approach loop closure	23
Figure 13: a) Displacement in x-direction of leaf from collimator centerline, b) two opposing four-bar linkages, and c) optimized dimensions for the linkage set.....	24

Figure 14: Isometric view of the four-bar linkage placement, a) is the placement of the linkage set one and two, b) is the placement of the linkage set three and four, and c) is the implementation of all four linkage sets.....	26
Figure 15: Implementation of for-bar linkage in CAD model.....	26
Figure 16: Leaf design and dimensions used in the SBIORT collimator.....	27
Figure 17: a) rapid prototyped SBIORT collimator, b) CAD model of SBIORT collimator's size with respects to a hand.....	28
Figure 18: a) experimental set-up used for position accuracy, b) image taken of the SBIORT collimator's aperture.....	30
Figure 19: Experimental set-up used in dosimetry measurements.....	32
Figure 20: Three-square shaped dose used to create step dose destitution.....	32
Figure 21: Data obtained from positional accuracy experiment of collimator opening size as a function of input angle with ± 0.25 mm error bars.....	34
Figure 22: Collimator approximately 100% open, a) dose distribution, b) dose profile use to determine transmission factor.....	35
Figure 23: Collimator approximately 100% open, a) dose distribution, b) dose profile use to determine penumbra value.....	35
Figure 24: a) dose distribution of a step dose pattern, b) the dose profile of the step dose pattern.....	36
Figure 25: Split gear used to reduce backlash in gears.....	38
Figure 26: The geometrical relationship between the focal spot size of a radiation source and the penumbra size.....	39

Chapter 1 - Introduction

There were an estimated 53,070 new pancreatic cancer cases in 2016 (3.1% of all new cancer cases). The overall 5 year-survival rate of pancreas cancer is 7.7%; this percentage has unfortunately not significantly improved in the last 25 years [1, 2]. Most pancreatic tumors are diagnosed in advanced stages of the disease, leaving the majority of patients with only months to live after diagnosis [3]. Surgical resection is the preferred method of treatment for tumors of the pancreatic head and neck; resulting in 5 year-survival rates in excess of 20% [4]. Though surgical resection remains the most effective therapeutic intervention, clear surgical margins are actually achievable in less than 20% of all cases [5]. The determining prognostic factors for resectable cases involve lymph node involvement, stage of infiltration into surrounding tissue, and presence of metastasis [6]. The most common method for removing tumors in the pancreas is the Whipple Procedure, or pancreaticoduodenectomy [4]. A standard Whipple Procedure involves the removal of the pancreatic head, gallbladder, duodenum (uppermost portion of the small intestine), pylorus (opening from stomach to duodenum), and the lymph nodes near the head of the pancreas. Pylorus preserving Whipple is a similar type of Whipple Procedure where the pylorus is not removed. The reconstruction involves connecting the pancreatic duct to the small intestine (Pancreaticojejunostomy), connection between hepatic duct and small intestine (hepaticojejunostomy), and connection of the stomach and the proximal loop of the small intestine (Gastrojejunostomy) [7]. Frequent local recurrence status post resection directly correlates to residual microscopic disease that is generally addressed with approximately 60 Gy of conventionally fractionated external beam radiation therapy (EBRT) [8]. Adjuvant radiotherapy confers a clear survival benefit [9]. However, EBRT

alone, does not achieve satisfactory tumor control, and is itself associated with various radiation induced normal tissue toxicities [10]. Trials with chemoradiation (500 mg/m² per day of 5-FU for 6 days and 40 Gy of radiation) following Pancreaticojejunostomy have demonstrated prolonged recovery in 24% of patients because chemoradiation could not be started until 10 weeks or more after surgical resection [11]. Thus, novel integrated therapies represent a vital strategy to improve pancreatic cancer outcomes [12].

1.2 Intraoperative Radiation Therapy

The feasibility of intraoperative radiotherapy (IORT) was demonstrated as early as 1905 by Comas and Prio [13]. Since then, various studies have continued to describe favorable effects of IORT in pancreatic cancer, which notably includes enhanced local control [14-16]. There are several practical advantages of IORT compared to EBRT. Most notably, IORT permits delivery of radiation directly to the tumor bed while it remains surgically exposed and thus maximizes the therapeutic ratio by selectively irradiating diseased sites. Healthy tissues can be further spared from radiation during surgery through the manual mobilization away from treatment fields, use of appropriate shielding, or selection of appropriate beam energies sufficient to limit dose to deep structures [14]. The immediate application of adjuvant radiation also addresses any residual microscopic disease which could regrow during post-operative convalescence time (weeks to months) required before EBRT can be administered. Additionally, because of the tight treatment field margins achievable by IORT, it offers great clinical value when treating tumors that are not addressable with EBRT due to nearby dose limiting tissues. For example, IORT is particularly applicable in pancreatic cancer where therapeutic EBRT dosing (for pancreas, 50.4 Gy delivered at 1.8 – 2 Gy/fraction) is constrained by the radiosensitive small bowel

or stomach. These advantages are further enhanced given IORT's unique ability to deliver very high doses of radiation (10 – 20 Gy) in single fractions [17], whereas to deliver the same biological effective dose via EBRT would require numerous fractions (all of which would also irradiate healthy uninvolved tissue). In this context, IORT and EBRT may even be used synergistically in a paradigm where a single high dose IORT application may reduce the total number of adjuvant EBRT fractions needed to achieve therapeutic effect.

However, due to the current technical limitations IORT [10, 18, 19], its clinical application in pancreatic cancer has been limited. These limitations include considerable size of treatment platform, prerequisite shielding requirements for operating rooms to ensure staff safety, inability to treat complicated tumor geometries, and lack of image guidance. For example, conventional electron-based IORT systems such as the Mobetron (IntraOp Medical Inc., Sunnyvale, CA) and LIAC (Sordina IORT Technologies (SIT) Inc., Vicenza, Italy) have relatively large footprints of 3.6 m³ and 2.9 m³, respectively, which can consume valuable operating room space. Though other IORT systems such as the NOVAC11 (Sordina IORT Technologies Inc., Vicenza, Italy), have 6 degrees of freedom in positioning the treatment beam, they are still unable to generate conformal radiation fields. Currently the method used to collimate the radiation dose in IORT is done with a tub-like applicator. The appropriate sized applicator is positioned manually around the targeted area, fixed rigidly in place, and the dose is delivered through the tube (shown in Figure 1) [20]. Applicators of various sizes and shapes can be used for IORT, however, the inability to dynamically collimate the radiation beam limits customizability of the treatment to irregular shape targets, resulting in potential over radiation of health tissue.

The treatment effects of healthy tissue can be better controlled with the implementation of conformal radiation therapy.



Figure 1: IORT applicator positioned in the surgical cavity of a patient with pancreatic cancer [20]

1.3 Objective for SBIORT

IORT delivers the dose directly to the tumor bed, decreasing the radiation effects of healthy tissue, and increasing the quality of life for the patient. Furthermore, treatment plans for post-surgical EBRT can be reduced with the implantation of IORT. Shielding requirements and maneuverability limit the implementation of IORT systems in surgical settings. In addition, current IORT delivery methods do not allow for the delivery of conformal radiation therapy in the surgical cavity. The objective in the development of the Scanning Beam IORT (SBIORT) system is to develop a compact image-guided IORT

system to improve upon IORT deliver methods by treating complex tumor geometries with a customized non-uniform radiation fields.

1.3.1 SBIORT Project

The compact SBIORT system is intended to be implemented on a mobile cart to be maneuvered within preexisting operating rooms. As shown in Figure 2 (a) and (b), SBIORT consists of a low energy x-ray source, a custom compact collimator module, a robotic arm, and a 3D surface-imaging module. The use of a low-energy photon source (50-70 kVp) in the SBIORT system would eliminate the need of costly shielding during operation. In addition, recent studies [21, 22] indicate that low-energy x-rays have a 20%-50% relative biological effectiveness (RBE) improvement relative to conventional high-energy x-rays. This enables an increase in clinical effectiveness in tumors, reducing the dose and therefore treatment time necessary to deliver the prescribed dose to the tumor bed. The 3D surface captured from the 3D surface imaging system is utilized for treatment planning and monitoring the surface motion during the radiation delivery. A compact dynamic collimation system is the essential component that provides the SBIORT system the ability to deliver conformal dose patterns to irregular shaped targets. The implementation of a collimation device in an IORT system involves development of such a device that is compact enough to maneuver within the surgical cavity while providing an adequately sized dose field. The development and implementation of a collimation device for the SBIORT system is essential to delivering conformal radiation therapy during IORT.

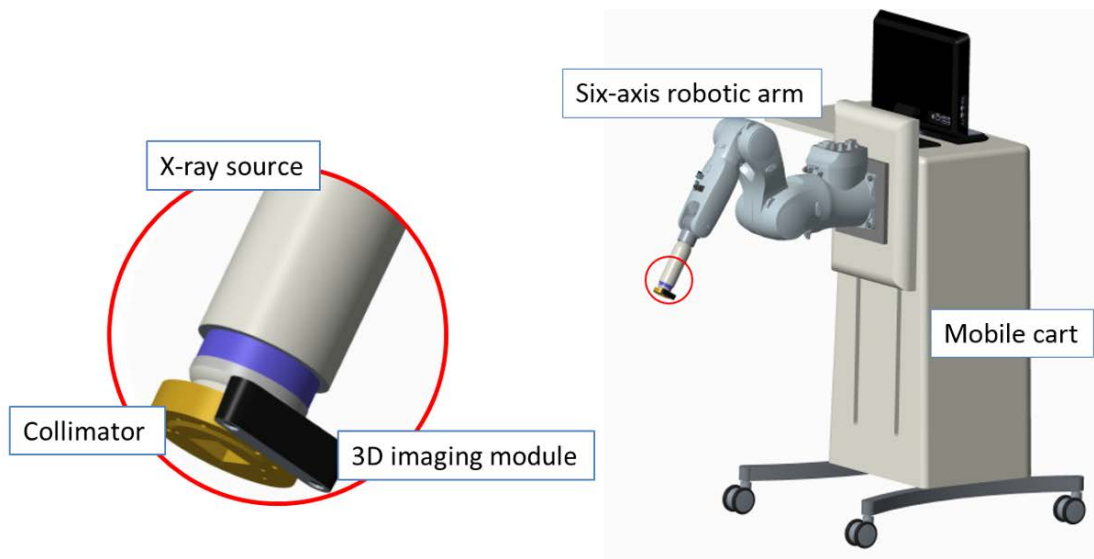


Figure 2: a) close-up of the of SBIORT system and b) model of SIORT system on mobile cart used to maneuver in surgical rooms. 3D scanning used to model the topography of the surgical cavity to be used in treatment planning process. The six-axis robot arm will maneuver the radiation source and collimator along the optimum path while the collimation system dynamically adjusts itself to effectively irradiate the desired region.

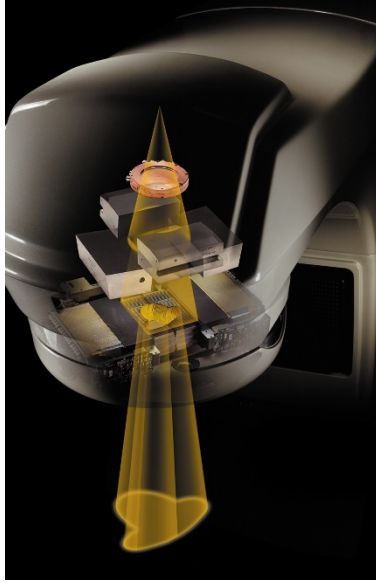
1.4 Collimation

Collimators are devices used to align the direction of particles or waves; collimators are also used to limit the cross sectional area of passing beams. Limiting the cross sectional area of a beam is the concept used in the control of visible light or exposer in photography and the basis for conformal radiation therapy. Conformal radiation therapy is a technique in which the radiation beam is collimated into the shape of a tumor or targeted region. Confining the radiation dose to the shape of the target, improves local control and reduces radiation effects on healthy tissue [23]. Three dimensional conformal radiation therapy (3DCRT) is a common practice in EBRT, which enables the radiation beam to be delivered to the tumor from various position around the patient. Collimation systems are utilized in (3DCRT) to conform the treatment volume to that of the tumor. The implementation of

precise collimation system provide the ability to deliver intensity-modulated radiation therapy (IMRT).

1.4.1 Multi-Leaf Collimator

EBRT can provide conformal radiation by utilizing a multi-leaf collimation (MLC) system. MLC can dynamically generate two-dimensional patterns used to collimate the radiation beam in the shape of a tumor (Figure 3 (a)). MLC is comprised of two banks of leaves on opposing sides of the device; each bank is comprised approximately 30-40 leaves and 1-2 cm in width (depending on the manufacture). The leaves move independently in linearly fashion to generate conformal dose patterns. The maximum field size of an MLC is 40 cm x 40 cm; each leaf can move 20 cm to the centerline of the MLC and an additional 10 cm, resulting in a maximum travel of 30 cm for each leaf [24]. The leaves are manufactured from various tungsten alloys, due to tungsten's relatively high density. MLC are capable of achieving precise dose profiles due to the device's ability to individually position each leaf, this equates to the system having a high number of degrees of freedom. Figure 3 (b) shows inner workings of a MLC; its respective actuator individually controls each tungsten leaf.



a)



b)

Figure 3: a) Radiation beam collimated with multi-leaf collimator and b) inside view of multi-leaf collimator [25]

1.4.2 Camera Shutter/Aperture

The investigation of additional collimation systems can be broadened towards devices that collimate visible light. A camera shutter is a device used in photography to allow light to pass through for given time intervals. The shutter is either in an open state or a closed state, the period in which the shutter is open determines the exposure time. The shutters are comprised of one or more moving opaque blades or leaves used to block the entrance of light into the camera [26-40]. Iris diaphragms are utilized in photography to control the amount of light entering the camera's lens. The opening size of the iris can be changed to regulate the amount of light entering the lens; as the opening is varied, the centerline of the opening remains positioned in line with the lens of the camera [41-50]. Iris style shutters have additional applications beyond camera optics; iris style valves can be implemented for flow control [51-55]. Analogous to keeping the light in line with the camera lens, an iris valve insures the centerline of the flowing mass is constant for various

opening sizes. Investigating collimation system designs implemented in applications outside of radiation therapy can be adapted and used in IORT, where currently no conformal radiation therapy is used.

1.5 Organization of the Document

This master thesis describes the development of the mechanical design for a compact collimation system intended for a novel SBIORT system for pancreatic cancer. In addition, manufacturing of collimator prototypes, positional accuracy, and dosimetry validation of the collimator design are discussed.

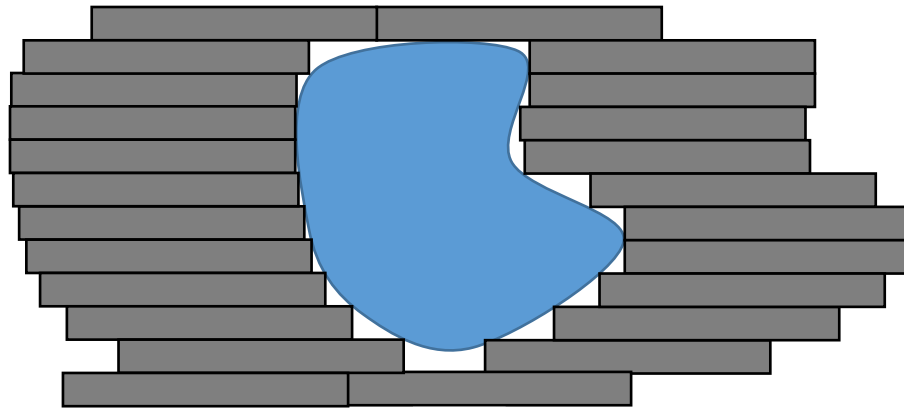
This document is organized into seven chapters. Chapter 1 presents the Introduction and motivation to develop a collimation system for SBIORT. Current IORT delivery procedures are investigated as well as alternative collimation systems used in application outside of radiation therapy. Chapter 2 discusses the design constraints for the SBIORT collimator system. Two collimation systems are investigated to determine the feasibility of implementing the designs in the SBIORT system. Chapter 3 presents the final design for the SBIORT system and discusses the dynamics of the mechanical design. Manufacturing and leaf design is also covered in Chapter 3. Chapter 4 discusses the validation of the collimator design in positional accuracy and dosimetry experiment. Chapter 5 presents the results from the position accuracy and dosimetry experiment. Chapter 6 provides a discussion on the SBIORT collimator design and the significance of the experimental results. Finally, Chapter 7 presents the conclusion for the development of the dynamic SBIORT collimation system.

Chapter 2 - Design Considerations SBIORT Collimator

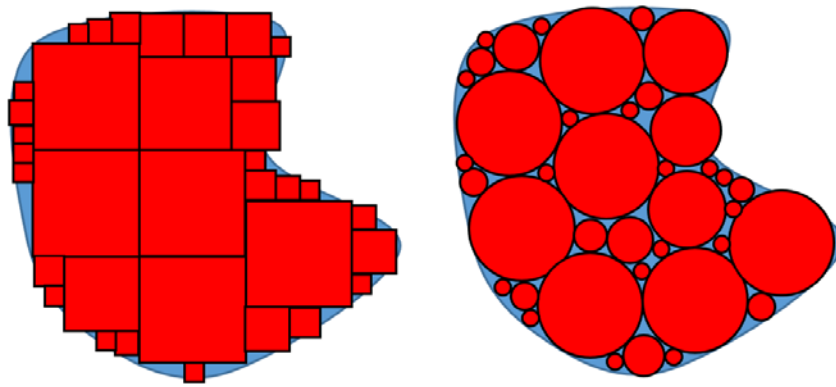
This chapter discusses the design constraints and processes used to develop a compact collimation system for an IORT system. The development of the IORT collimation system involved the consideration of preexisting collimation systems used in applications outside of radiation therapy. The first design consideration is of an MLC system used for conformal radiation therapy for EBRT. The second design consideration is that of an iris aperture used to collimate light in photography. The two design considerations were analyzed to determine the feasibility of implementation in SBIORT system.

2.1 Design Objectives and Constraints

The main object of the SBIORT collimation system is to conform the radiation beam to the shape of the tumor; this can be done similar to an MLC system used in EBRT, where the leaves individually move to generate a 2-dimensional pattern of the tumor (Figure 4 (a)). Alternatively, the IORT collimation system can generate conformal radiation by delivering a series of various sized doses, which when aliened, cover the entirety of the tumor; this multiple dose treatment method can be represented with a packing scenario shown in Figure 4 (b), where the blue region represents an arbitrary tumor area and the red is the does delivered. There are approximately the same number of squares and circles in Figure 4; however, the squares provide a more uniform coverage without having to overlap doses.



a)



b)

Figure 4: a) 2-dimensional pattern generated by a MLC to conform to tumor shape and b) comparison of geometric packing of an arbitrary shape using squares vs circles

Implementing a collimation device in SBIORT system requires the device to be compact in order for it to maneuver within the surgical cavity (surgical cavity being approximately 10-15 cm in diameter). Transversely, the field size or maximum dose area of the device must be large enough to effectively treat the tumor in an adequate time frame to be implemented in the surgical procedure. A square collimator field size of 20 mm by 20 mm would result in a treatment time of approximately 40 min with 1 cm radiation depth on a tumor of 6 cm in diameter. Similar to the manufacturers' specification of commercially used MLC systems, the transmission through the leaves of the SBIORT collimation system

was desired to be 0.5% or less [56]. The precision of the leaves position was desired to be less than 0.5 mm. The design constraints discussed in this section were used to determine the feasibility of design concepts.

2.2 Multi-Leaf Collimator Design

In the early stages of designing a collimation system for the SBIORT system, it was desirable to investigate the possibility of implementing an MLC-like device due to its widely used application in conformal radiation therapy in EBRT. The MLC designed for the SBIORT system was a scaled down version of a standard sized MLC system used on the linear accelerators. The design involved two banks of 10 leaves (20 total leaves) with each leaf 2.6 mm wide, providing a maximum field size of 30 mm x 26 mm. Similar to a standard MLC, each leaf of the SBIORT MLC needed to be controlled individually. In a standard MLC system, the motion of the leaves are controlled by an actuator, placed behind each leaf, as shown in Figure 3 (b). However, the placement of actuators in the IORT MLC could not be configured in this fashion, due to size limitations discussed in the above section. The individual control of leaves in a standard MCL is not a major issue when analyzing the device's overall size; a standard MLC is not design to be implemented in a surgical cavity unlike the SBIORT MLC. The SBIORT collimator was designed such that the linear actuators would be placed above the leaf banks to reduce the collimator's cross sectional size at the base, to enhance maneuverability within the surgical cavity. Figure 5 (a) shows the placement of the linear actuators above the leaf bank, the vertical motion of the actuator would be translated into horizontal motion with use of an L-shaped linkage. The L-shaped linkage design was optimized to determine the smallest possible cross-section at the base of the SBIORT MLC; this would involve optimizing linkage L_1 and L_3

in Figure 5 (a). The optimization of linkage L_1 and L_3 was performed by solving the two linkages' characteristic equations as function of linkage L_2 . Equation 1 and Equation 2 can be written for linkages L_1 and L_3 , respectively; Equation 3-Equation 7 are used to write Equation 2 (L_3) as function of L_2 . The variable x denotes half the leaf's desired displacement and the variable γ is used as the angular limitations of the pivot point between the leaf and linkage L_3 . The values of L_1 and L_3 were graphed as a function of L_2 to determine the optimal lengths, as shown in Figure 6. The optimal lengths of the L-shaped linkage is indicated by the interception of linkage lengths L_1 and L_3 in Figure 6.

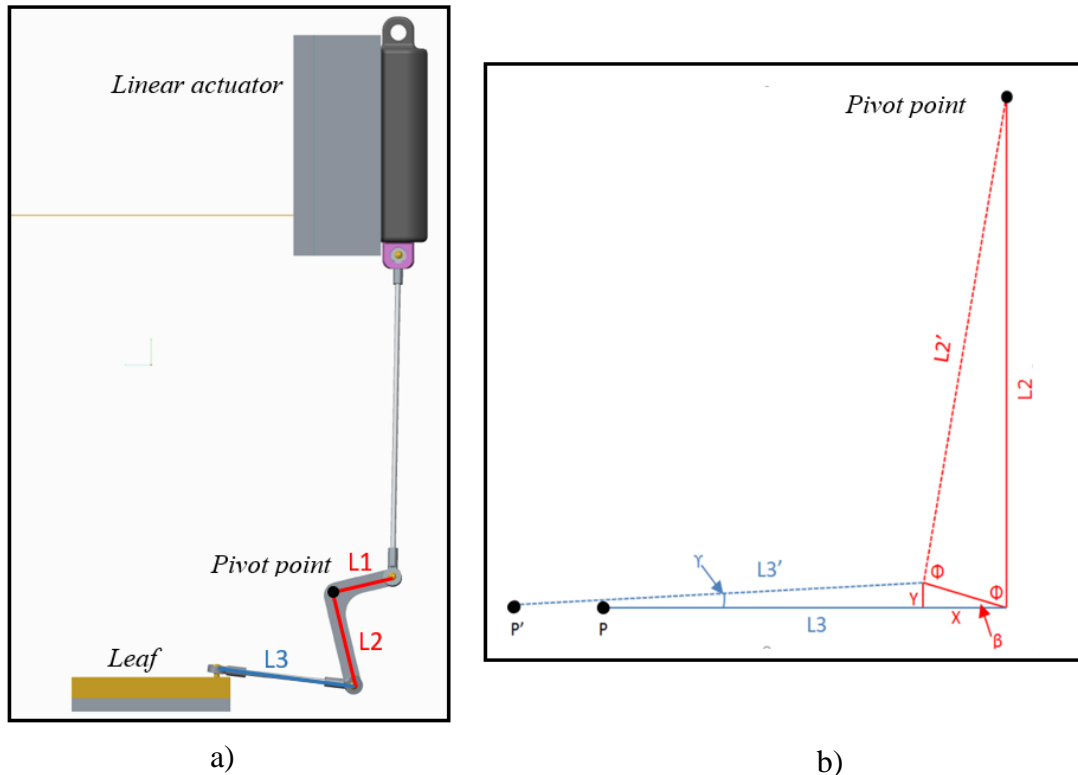


Figure 5: a) SBIORT MLC linkage design and b) linkage optimization parameters

$$L_1 = \frac{L_2}{1.5} \quad \text{Equation 1}$$

$$L_3 = \frac{y}{\sin \gamma} \quad \text{Equation 2}$$

$$\beta = 90 - \phi \quad \text{Equation 3}$$

$$\phi = \frac{(180 - \theta)}{2} \quad \text{Equation 4}$$

$$\theta = \cos^{-1} \left(-\frac{x_2^2 - 2 * L_2^2}{2 * L_2} \right) \quad \text{Equation 5}$$

$$y = x_2 \sin \beta \quad \text{Equation 6}$$

$$x_2 = (y^2 + x^2)^{\frac{1}{2}} \quad \text{Equation 7}$$

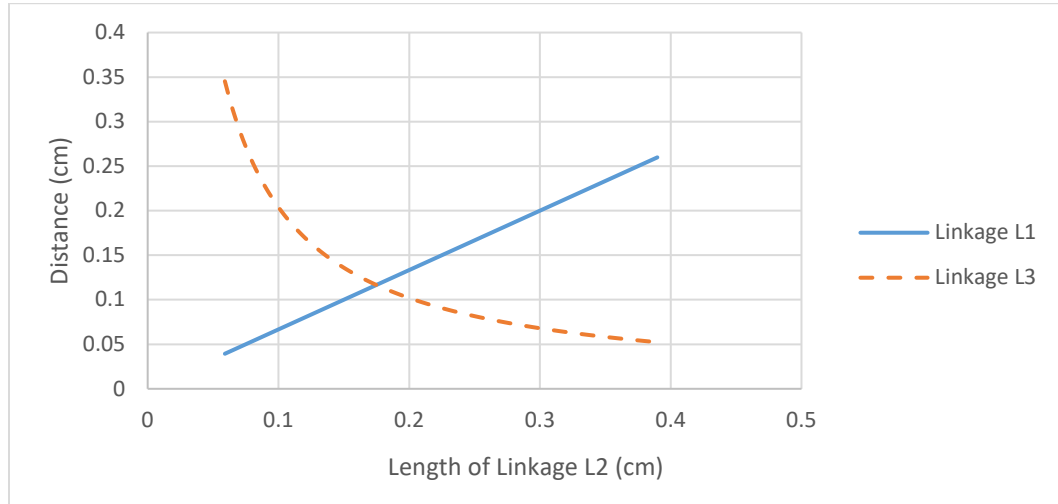


Figure 6: SBIORT MLC linkage optimization

2.2.1 Conclusion: Multi-Leaf Collimator Design

Despite large application of MLC devices in EBRT, the design was not suitable for IORT. The MLC design would provide highly conformal doses with 20 degrees of freedom; however, after optimizing the design, the SBIOT MLC system could not be

produced with a cross section smaller than 13.0 cm. The cross-sectional size is a result of doubling the summation of the optimized linkages L_3 and L_1 (approximately 0.116 cm) with the length of the leaf (approximately 3.0 cm) and half the opening size (1.0 cm). A cross section of 13.0 cm would not be compact enough to properly fit or maneuver within the surgical cavity.

2.3 Iris Diaphragm Shutter

An iris diaphragm shutter was investigated to determine the feasibility of implementing the design in a SBIORT collimation system. The objective is to utilize the iris shutter's dynamically adjustable blades to generate conformal radiation by delivering a series of various sized doses. The iris shutter is comprised of two discs, the bottom disc is fix while the top disc is able to rotate about the centerline; the rotation of the top disc allows the blades to open and close the aperture. Figure 7 shows a six-blade iris diaphragm as it is opened in three different stages. The clockwise rotation of the transparent top disc forces the blades move in the groves cut on the disc, as the blades move along the groves, they rotate about pivot points on the bottom disc. Figure 7 shows an isometric view of the iris shutter, in the images the blades are stacked on top of one another to allow them to slide freely without colliding into one another.

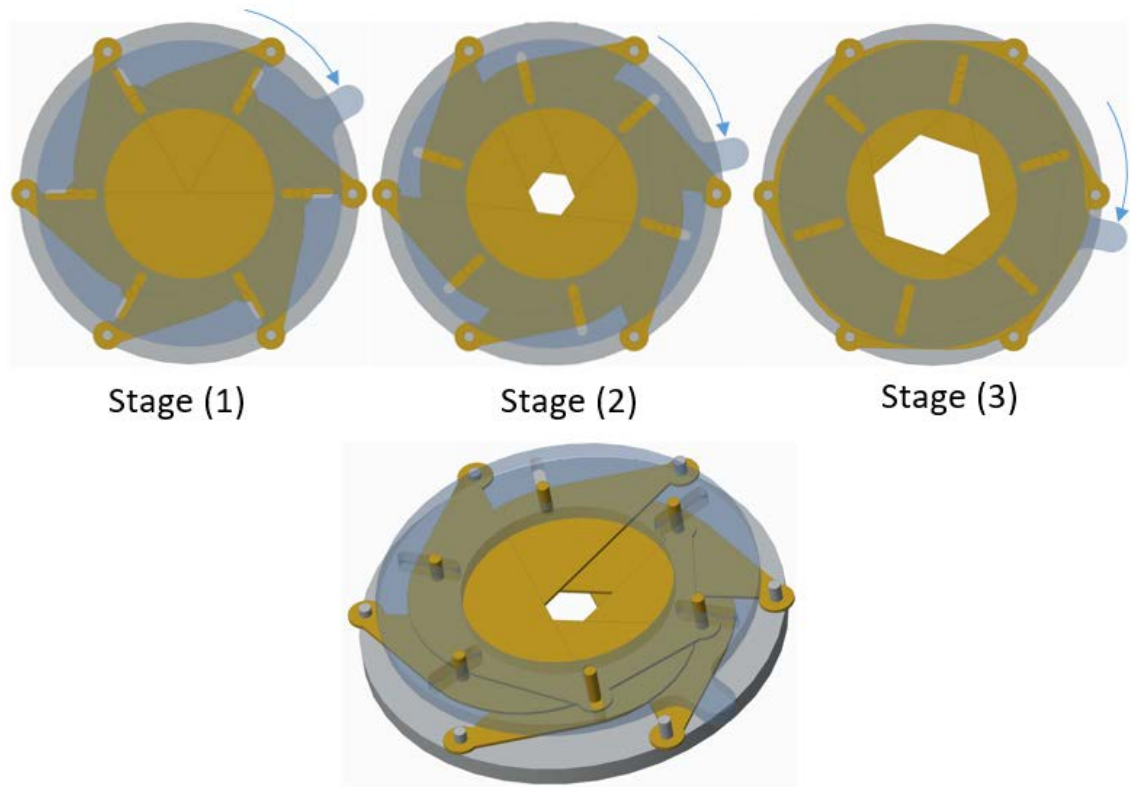


Figure 7: Six-blade iris diaphragm cycled from a closed state to open (Stage 1-3) and an isometric view (bottom)

There is a variety of iris blade geometries for various application; in most applications, the blades have a curved geometry to generate an approximate a circular aperture. As discussed in the section 2.1 of this paper, it was desirable to design a collimation system that provided a variable square shaped aperture, to better alien doses within the same target zone. If the six-blade iris shutter from Figure 7 was reconfigured to a four-blade iris, it would provide a variably square aperture. However, as the size of the aperture was varied, the square shape would rotate with respects to the bottom fixed disc. As the hexagonal shape in Figure 7 is increased in size from state (2) to state (3), the

hexagon is rotated clockwise. Not having a constantly oriented aperture shape presents additional requirements to control the position of the collimation system.

Alternative designs of the iris shutter were investigated to eliminate the rotation of the aperture shape, as it was cycled open and close. The design in Figure 8 shows a shutter similar to the original iris shutter, however, this design utilizes a gear system to rotate both discs equally and in opposite directions. This collimation system has one degree of freedom, allowing the aperture size to be controlled with one rotational input on either of the gear shafts.

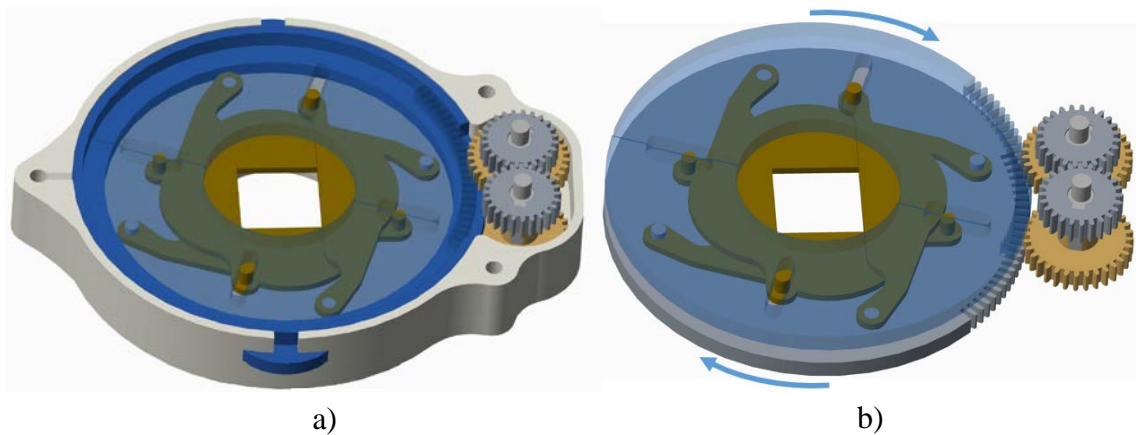


Figure 8: Alternative iris shutter design with two counter-rotating discs, a) with a cover, and b) without cover

Kinematic loop closure equations were applied to the alternative iris shutter to quantify the blade's rotation with respects a fixed origin. Figure 9 (a) shows the kinematic linkages overlaid on the CAD drawing of the alternative iris shutter. The center pivot point of the linkages are displayed as a fixed position; this represents the cover or housing of the shutter. Linkage R_1 is the distance from the blade's pivot point on the bottom disc to the centerline of both discs. Linkage R_2 represents the length of the blade. Linkage R_3 is the distance from the blade's position in the top disc's groove to the centerline of both discs, the

length of R_3 changes as the aperture is rotated and this implies R_3 is a function of the input angle. Vectors R_1 , R_2 , and R_3 are aligned in a closed loop, Equation 8 can be written as the summation of vectors in a closed loop equal zero. Equation 8 can then be split into the x and y components of each vector to generate Equation 9 and Equation 10. To understand the angular position of the blade (θ_2), Equation 9 and Equation 10 are solved for R_3 and θ_2 , respectfully to provide Equation 11 and Equation 12. Given that the rotation of the two discs are equal and opposite, Equation 13 can be written to express the relationship between θ_1 and θ_3 . Equation 11 and Equation 12 were iteratively solved to graph the position of the blade (θ_2) with as a function of the blade moving across the opening, shown in Figure 10.

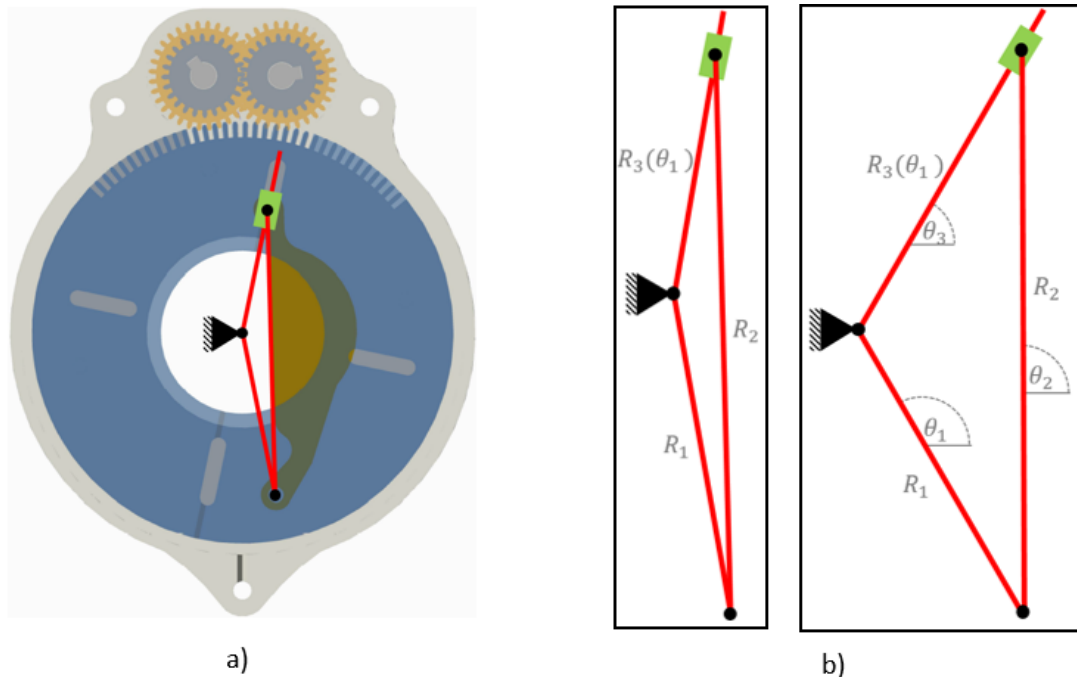


Figure 9: Kinematic analysis of alternative iris shutter design with two counter-rotating discs, a) the kinematic linkages overlaid on the CAD drawings, and b) the linkage system at two separate positions

$$\sum_{i=1}^3 R_i = \vec{R}_1 + \vec{R}_2 + \vec{R}_3 = 0 \quad \text{Equation 8}$$

$$\text{X-direction: } R_2 \cos \theta_2 - R_3 \cos \theta_3 - R_1 \cos \theta_1 = 0 \quad \text{Equation 9}$$

$$\text{Y-direction: } R_2 \sin \theta_2 - R_3 \sin \theta_3 - R_1 \sin \theta_1 = 0 \quad \text{Equation 10}$$

$$\theta_2 = \cos^{-1} \left[\frac{R_3 \cos \theta_3 + R_1 \cos \theta_1}{R_2} \right] \quad \text{Equation 11}$$

$$R_3 = \left[\frac{R_2 \sin \theta_2 - R_1 \sin \theta_1}{\sin \theta_3} \right] \quad \text{Equation 12}$$

$$\theta_1 = 180 - \theta_3 \quad \text{Equation 13}$$

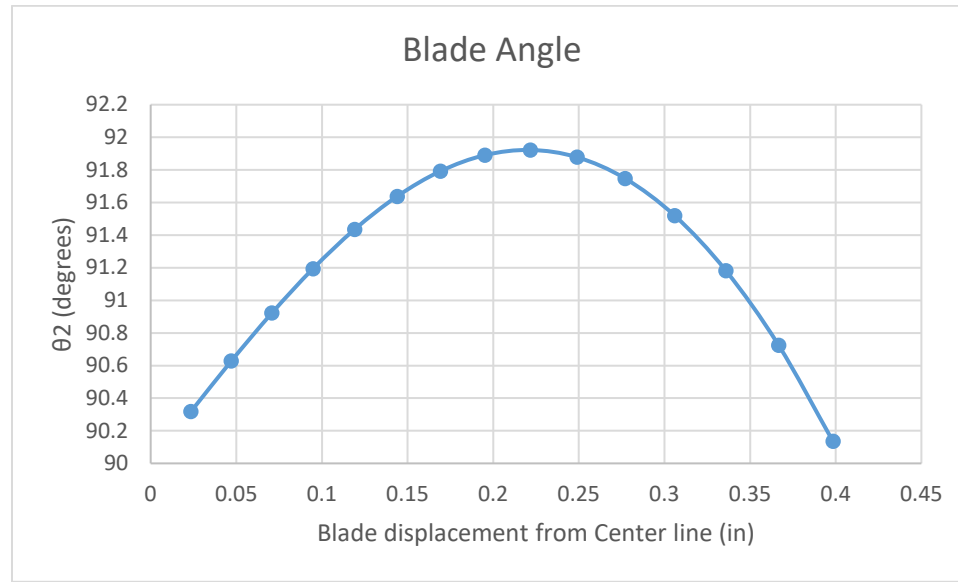


Figure 10: Angular position of the alternative iris blade as it is cycled open

2.3.1 Conclusion: Iris Diaphragm Shutter

The compacted size of the iris shutter is adequate to be implemented in the SBIORT system. Even with the implementation of the second rotating disc, the angular position of the blades would not remain at a constant position with respects to the centerline of the collimator as the aperture was cycled open and close. Since the angular position of the

blades can be quantified as a function of the input angle to the shutter, a possible solution to overcome the blades rotation could be to rotate the entire shutter with a robotic platform as the shutter is in use. However, the additional controlling constraints of the alternative iris shutter did not make the design ideal for the implementation in the SBIORT system.

Chapter 3 - SBIORT Collimation Design

This section discusses the details of the final SBIORT collimation design and the manufacturing of prototypes. The investigation of alternative designs discussed in Chapter 2 lead to the final SBIORT collimation design consisting of shutter mechanism to achieve a small sectional area in order to maneuver within the surgical cavity, which was not obtainable by manipulating MLC designs. To avoid the blade rotation discussed in the 2.3 *Iris Diaphragm* Shutter section, a shutter design with an addition linkage was considered. The motion of the iris blade can be characterized by a three-bar linkage system involving a slider (Figure 9), the SBIORT shutter design utilizes a four-bar linkage system, shown in Figure 11. The patent-pending dynamic collimator design is comprised of four leaves that move in unison to create a variable square aperture used to shape the radiation beam.

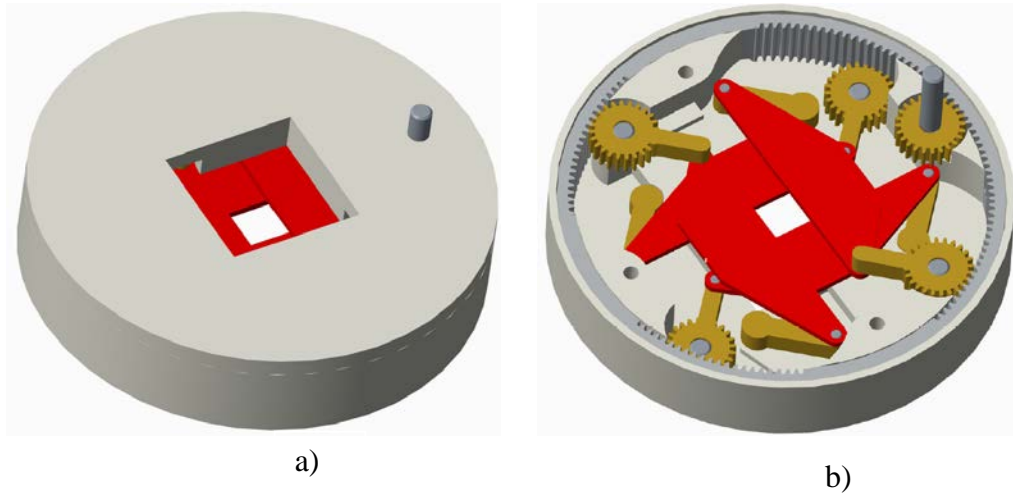


Figure 11: Patent pending dynamic collimator design, a) with top cover on, and b) without top cover

3.1 Dynamics of Collimator Design

The collimator design utilizes four leaves to create the square shaped aperture. The motion of each leaf can be characterized by a planar four-bar linkage; in which member L_2 in Figure 12 (a) represents the leaf and member L_4 represents the housing of the collimator. The four-bar linkage has one degree of freedom, allowing for the position of the leaf or member L_2 to be defined by a single rotational input at any of the four pivot points (Figure 12 (a) displays the rotation at the joint between L_1 and L_4). Constraining opposite members to be equal in length ($L_1=L_3$ and $L_2=L_4$) creates a parallelogram and insures member L_2 will remain parallel to a given origin (Figure 12 (a) and (b)). Keeping member L_2 or the leaf from rotating overcomes the issues faced in the iris design. A kinematic loop closure approach provides the equations of motion for the planar four-bar linkage. Representing the members of the linkage as vectors (Figure 12 (b)) provides Equation 14, where the summation of vectors in a closed loop equal zero. Each vector can be broken down into an x-component and y-component; Equation 14 can then written as Equation 15 and Equation 16, using the angles denoted in Figure 12 (b).

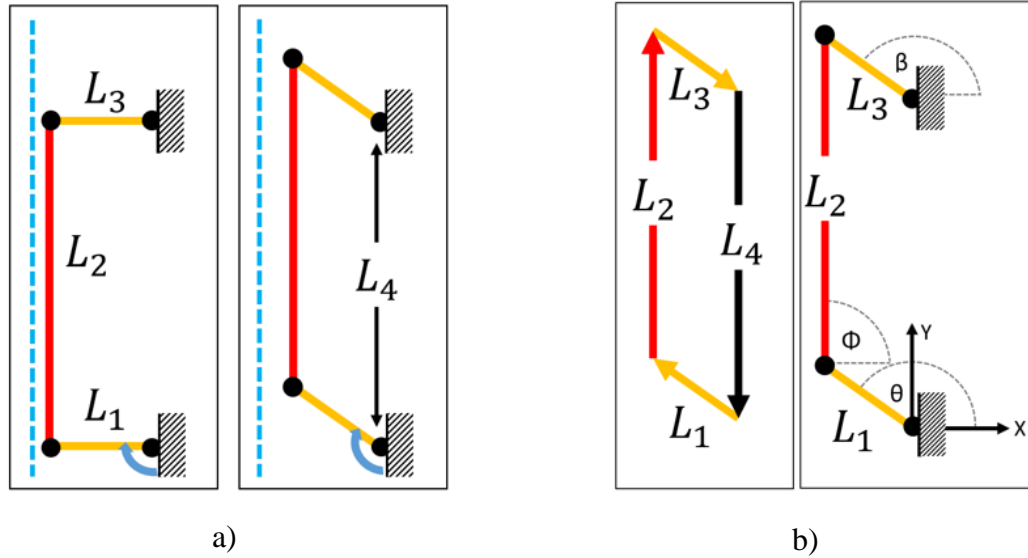


Figure 12: a) Planar four-bar and b) kinematic approach loop closure

$$\sum_{i=1}^4 L_i = \vec{L}_1 + \vec{L}_2 + \vec{L}_3 + \vec{L}_4 = 0 \quad \text{Equation 14}$$

$$\text{X-direction: } L_1 \cos \theta + 0 - L_3 \cos \beta - 0 = 0 \quad \text{Equation 15}$$

$$\text{Y-direction: } L_1 \sin \theta + L_2 - L_3 \sin \beta - L_4 = 0 \quad \text{Equation 16}$$

3.2 Optimizing Size

As mentioned above, it was critical the overall size of the collimation device remain as small as possible, to insure the device can maneuver effectively inside the surgical cavity. Optimization performed on the kinematic equations aided in determining the smallest linkage needed to achieve a field size of 20 mm x 20 mm. The field size or the opening of the aperture is defined by twice displacement in the x-direction of a leaf; this is shown in Figure 13 (a), where the blue line represents the centerline of the collimator. Implementing two opposing four-bar linkages (Figure 13 Figure 12 (b)) creates the full field (represented by dashed line in Figure 13 (b)) size, where twice ΔX equals the aperture

opening. The displacement in the x-direction is determined from Equation 17; Equation 17 is the kinematic equation of motion for the leaf and it is the first portion of Equation 15. Setting the Equation 17 equal to half the desired field size (10 mm) and limiting θ between $90^\circ - 180^\circ$ (90° is a closed aperture state and 180° is a fully open state) the optimal linkage lengths can be determined as $L_1=L_3 = 10$ mm. As the linkage set is rotated opened (θ approaches 90°); linkage L_2 is moved upwards with respects to the window opening, resulting in the optimal length for linkage L_2 and L_4 is 30 mm (10 mm+ 20 mm), as shown in Figure 13 (c).

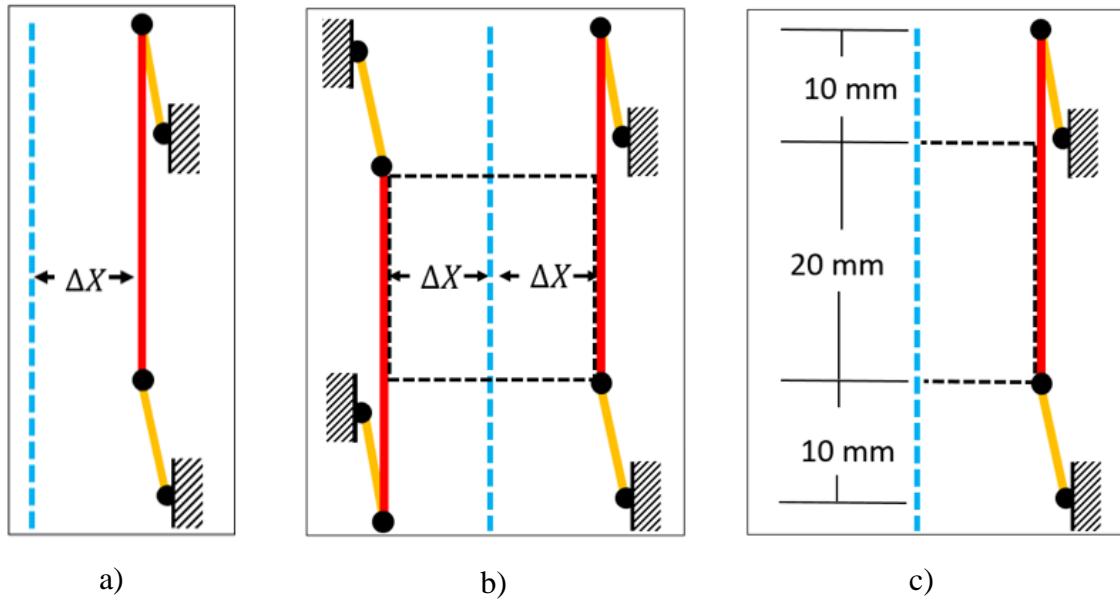


Figure 13: a) Displacement in x-direction of leaf from collimator centerline, b) two opposing four-bar linkages, and c) optimized dimensions for the linkage set

$$L_1 \cos \theta = \Delta X \quad \text{Equation 17}$$

3.3 Developing Design

In order to create a variable square opening, the collimator is comprised of four sets of planar four-bar linkages. Figure 13 (b) shows the placement of a second four-bar linkages rotated 180° from the first; the same process is done to implement the third and

fourth linkages; however, the third and fourth leafs must be placed just above the first two sets. Linkage sets one and two are then able to slide underneath linkage sets three and four. Figure 14 shows an isometric view of the four-bar linkage placement; linkage set three and four (Figure 14 (b)) is raised 1.0 mm (thickness of the leaf) above the first two linkage sets (Figure 14 (a)). Figure 14 (c) shows the placement of the four linkage sets used to construct the square shaped aperture. A collimation system comprised of four separate four-bar linkages has four degrees of freedom; meaning, it would require four separate inputs to control each linkage set to form a variable square opening. It was desirable to decrease the number of degrees of freedom in order to reduce and simplify the controls of the collimation system. A gear system was used to couple the four linkages together to reduce the degrees of freedom to one for the entire collimation system. Each L_1 member is composed of a spur gear centered on the pivot point, allowing the four linkage sets to be coupled together with the implementation of an internal spur gear, as shown in Figure 12 (b) and Figure 12 (c). Coupling the linkage sets together allows the collimator system to have one degree of freedom, therefore, the aperture size to be controlled by a single radial input.

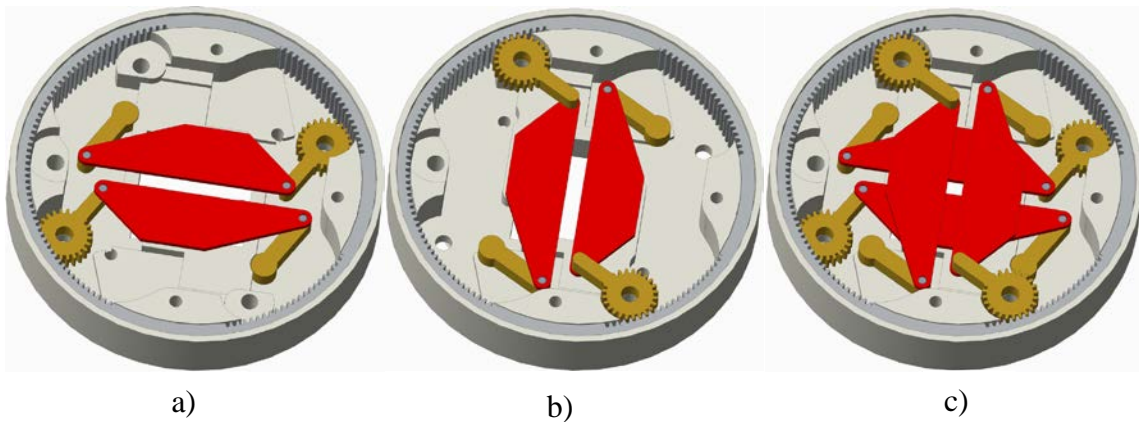


Figure 14: Isometric view of the four-bar linkage placement, a) is the placement of the linkage set one and two, b) is the placement of the linkage set three and four, and c) is the implementation of all four linkage sets

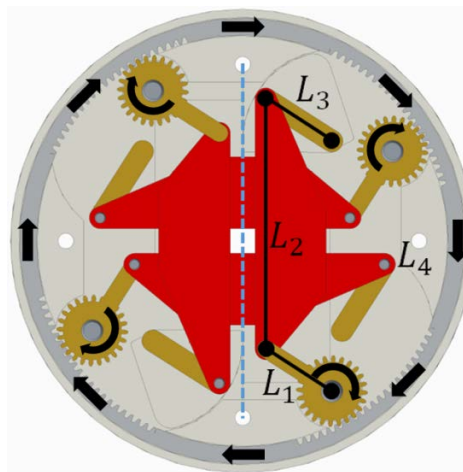


Figure 15: Implementation of for-bar linkage in CAD model

3.3.1 Leaf Design

The four leaves of the of the SBIORT collimator are used to conform the radiation beam to the shape of the tumor. The leaves were designed to have a transmission factor of less than 0.5%, as discussed in section 2.1. The leaf was designed to be manufactured out of tungsten. Tungsten is used for leaf construction in MLC systems, due to the materials ability to attenuate (weaken) the radiation beam. The variable I in Equation 18 denotes the

intensity of photons transmitted through a distance x of the leaf, μ is the linear attenuation coefficient of tungsten and I_0 is the initial intensity of the photon. From Equation 18, it was determined a leaf thickness of 1 mm would provide an adequate transmission factor for the given radiation source of 50 kPv.

$$I = I_0 e^{-\mu x} \quad \text{Equation 18}$$

The optimized size of the leaf was determined as 30 mm in length and a width of 10 mm, as discussed in section 3.2. However, leaf dimensions had to be adjusted when implementing into the SBIORT collimator. The dimensional changes were necessary to insure the leaf's pivot joints remained clear of the radiation beam. After manipulating the optimized leaf dimensions, the final leaf length measures 36.3 mm and a leaf width of 10.7 mm as shown in Figure 16.

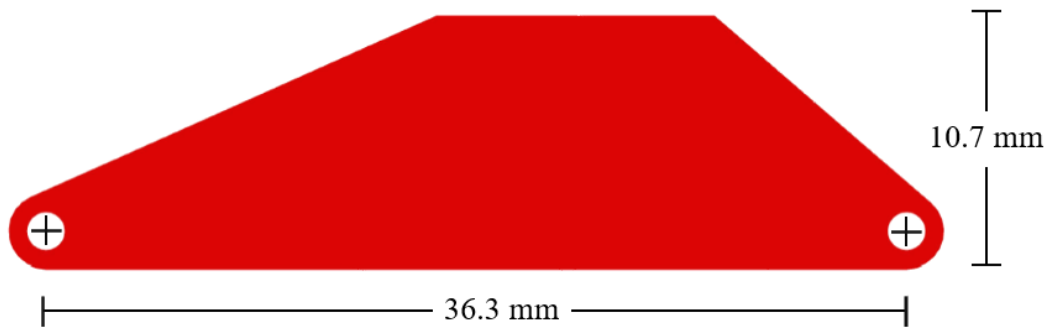


Figure 16: Leaf design and dimensions used in the SBIORT collimator

3.4 Manufacturing Prototypes

SBIORT collimator prototypes were manufactured to validate its functionality of the mechanical design. The prototype (Figure 17 (a)) were manufactured using fused

deposition rapid prototype printers. The material used in the printing process was Acrylonitrile butadiene styrene (ABS), which was printed at a resolution of 0.005". Opposed to printing the pins used of the picot joints, stainless steel dowel pins were pressed into the spur gears to decrease rotational resistance. The leaves were manufactured out of 1 mm thick copper tungsten alloy using of conventional milling processes. Copper tungsten alloy was the preferred material due to its manufacturability compared to other tungsten alloys.



Figure 17: a) rapid prototyped SBIORT collimator, b) CAD model of SBIORT collimator's size with respects to a hand

Chapter 4 - Experimental Validation

The SBIORT collimator was validated experimentally to ensure the mechanical design of the device would perform as intended. An experiment was conducted to quantify the device's positional accuracy capabilities. Dosimetry measures were conducted to determine the collimator's penumbra and transmission values as well as validate the device's capability to deliver step dose distributions.

4.1 Collimator Position Accuracy Test

The collimator positional accuracy study was performed to determine the positioning accuracy of the collimator leaves. An Image processing method was applied to measure the leaf's displacement. Other displacement measuring methods requiring physical contact from a measuring device (caliber, digital indicator, coordinate measuring machine, etc.) can remove backlash in the collimation system, resulting in inaccurate values that would not represent the accuracy of the device for how it is intended to be used. In the experiment, a rotary quadrature encoder was mounted on the collimator to measure the radial input, a high resolution NX4-S2 camera (Integrated Design Tools, Tallahassee, FL) was placed orthogonally above the collimator to capture images of the collimator opening (Figure 18). The camera remained at the same distance from the collimator for each measurement to insure the images had the same pixel size. A light was used underneath the collimator to illuminate the aperture open; this aided in the processing stage by supersaturating the opening in the images. Up-scale repeatability measurements were performed by manually opening the collimator to measured inputs of 30°, 50°, and 75° from the rotary encoder (an input of approximately 80° results in the collimator at a fully open state). Once the collimator was opened to the desired input, the camera captured

images of the leave's position, this was repeated eight times for each set of radial inputs. A calibration curve was obtained by collecting eight measurements across the opening range ($0^\circ - 80^\circ$) of the collimator.

A MATLAB (MathWorks, Natick, MA) program was used to process the images. The pixel size of the images was computed by referencing a known object in the images. The program measured the aperture opening by summing the pixels linearly between leaves the converting the number of pixels to millimeters.

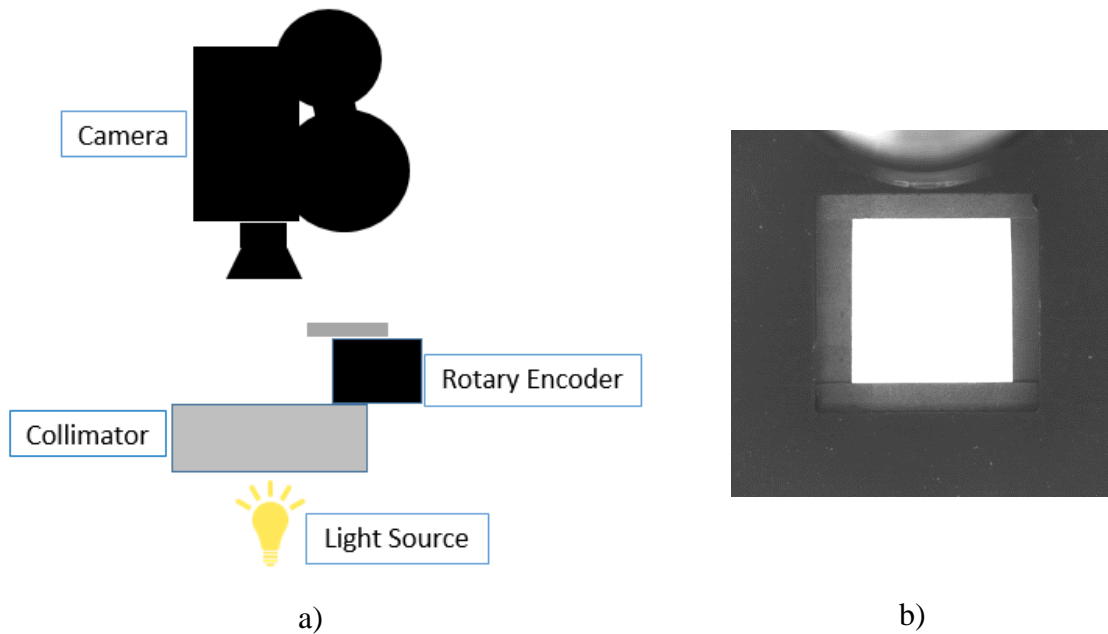


Figure 18: a) experimental set-up used for position accuracy, b) image taken of the SBIORT collimator's aperture

4.2 Dosimetry Experiment

The objective of performing dosimetry experiments on the SBIORT collimator prototype (Figure 18 (a)) was to determine the penumbra value and transmission factor of the device and demonstrate the design can deliver intensity modulated doses using a step

dose distribution. In the experiment, a 50 kVp x-ray source was simulated using a low-energy x-ray unit (Pantak DXT-300, Pantak Pty Ltd, East Haven, CT). The experimental set-up used in the dosimetry measurements is displayed in Figure 19. To create a step dose pattern, the collimator was positioned 35 cm (D_1 in Figure 19) below the x-ray source and EBT3 radiochromic film was used at a distance of 10 cm (D_2 in Figure 19) underneath the collimator to measure the collimator dose distribution, following TG-61 recommendation [57]. The step dose pattern was achieved by delivering two square doses side-by-side and a third dose in the middle of the first two; the positioning of the three doses can be seen in Figure 20. The dosimetric penumbra value was obtained with the collimator approximately 100% open, 25 cm (D_1 in Figure 19) below the x-ray source, and 10cm (D_2 in Figure 19) above the radiochromic film, 7 Gy was delivered at the film. Similarly, the transmission factor was obtained with the collimator at approximately 100% open and positioned 10 cm above the radiochromic film (D_2 in Figure 19).

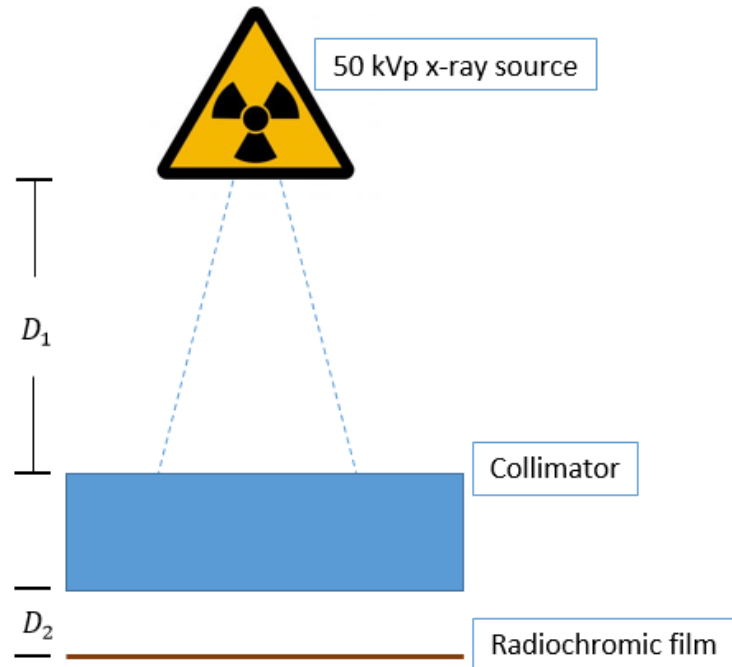


Figure 19: Experimental set-up used in dosimetry measurements

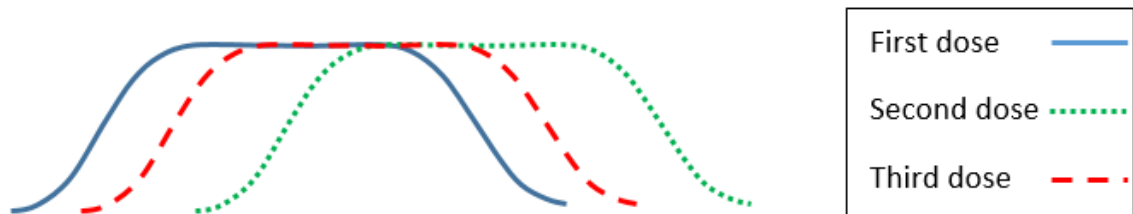


Figure 20: Three-square shaped dose used to create step dose destitution

Chapter 5 - Experimental Results

The positional accuracy, penumbra value, and transmission factor were determined and step dose distribution were demonstrated for the SBIORT collimator prototype. This section discusses the results from the positional accuracy and dosimetry experiments conducted on the collimator prototype.

5.1 Collimator Positional Results

The collimator positional accuracy was determined using the up-scale repeatability and the calibration curve fit. The accuracy of the rotary encoder and pixel size of the camera were added in quadrature to generate the experimental bias error. The upscale repeatability measurements at input angles of 30°, 50°, and 75° and the third order polynomial regression analysis on the calibration curve was used to calculate an experimental precision error. The precision and bias errors resulted in a total uncertainty of the collimator to be ± 0.25 mm, at a 95% confidence interval. The calibration curve obtained from the experiment is displayed in Figure 21, with ± 0.25 mm error bars.

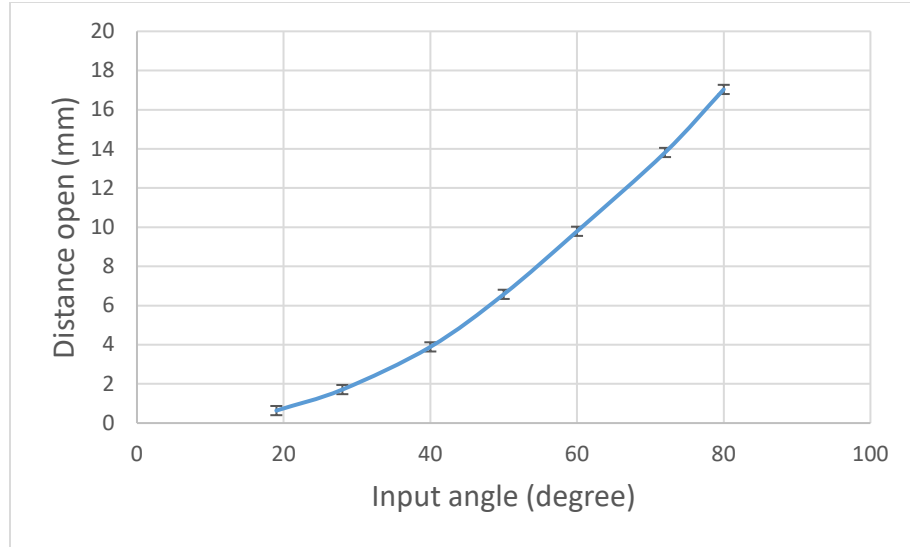


Figure 21: Data obtained from positional accuracy experiment of collimator opening size as a function of input angle with ± 0.25 mm error bars

5.2 Dosimetry Results

The radiochromic film from the dosimetry experiment were processed using MATLAB multi-paradigm numerical computing software. Figure 24 shows the step dose pattern using the collimator prototype, resulting is a maximum dose of approximately 5 Gy. The penumbra of the collimator was determined to be 1.9 mm and the transmission factor of the leaves was 0.5%.

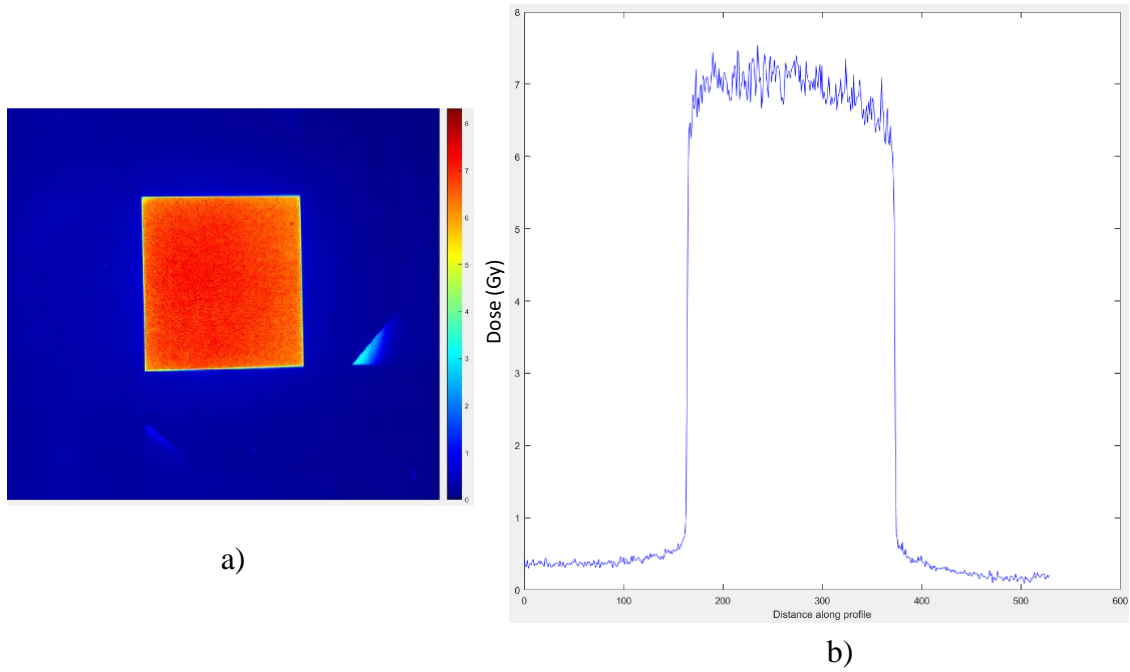


Figure 22: Collimator approximately 100% open, a) dose distribution, b) dose profile use to determine transmission factor

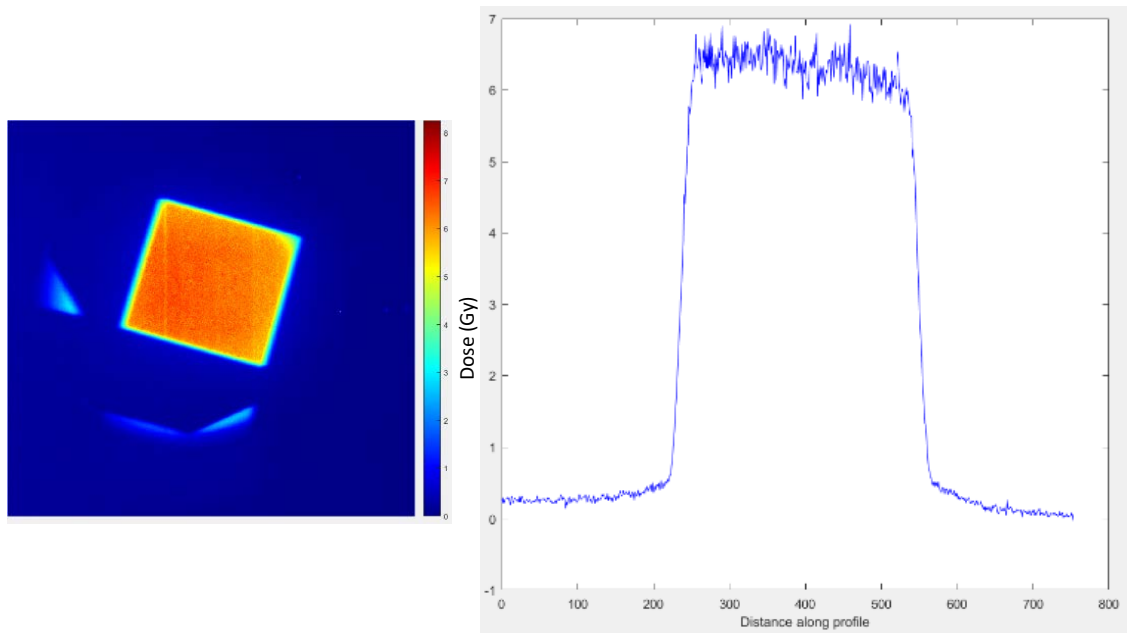
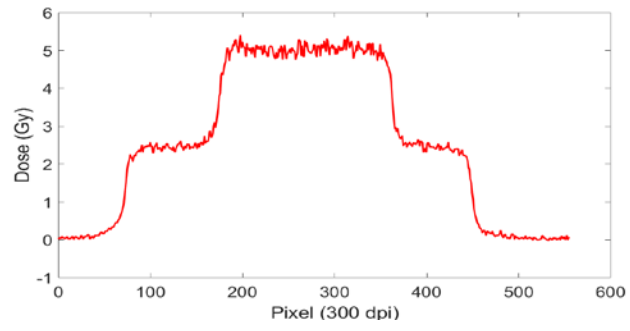
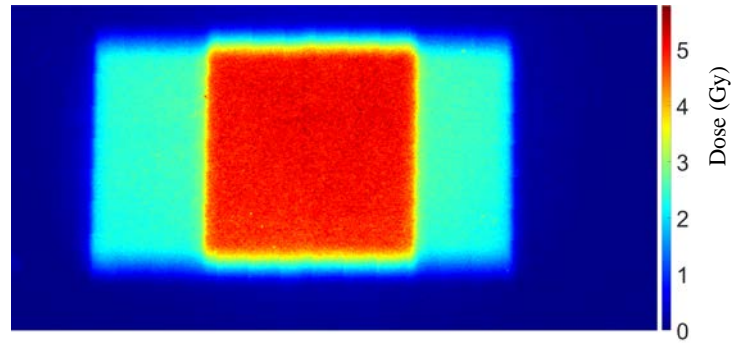


Figure 23: Collimator approximately 100% open, a) dose distribution, b) dose profile use to determine penumbra value



a)



b)

Figure 24: a) dose distribution of a step dose pattern, b) the dose profile of the step dose pattern

Chapter 6 - Discussion and Considerations

This section discusses the SBIORT collimator design, design considerations, and the significance of the experimental results.

6.1 Discussion Collimator

The SBIORT collimator design is a viable way to deliver intensity modulated intraoperative radiation therapy. The collimator's compact design has an approximate outside diameter of 66 mm, allowing it to maneuver within the surgical cavity. The collimator would be able to deliver a prescribed dose to a 6 cm diameter surface in approximately 40 min, making it a suitable time frame to be implemented during surgical procedures.

The design of the collimator is based on a four bar kinematic system as stated above in Chapter 3. The relationship between the input of the collimator and the displacement of a leaf can be represented with a third order polynomial equation. The nonlinear relationship between input and leaf displacement results in an inaccurate positioning of the leaves when the shutter opening size is less than approximately 2 mm. The inability to achieve small opening sizes of 2mm and less is not detrimental to the collimator design, since there is not a clinical need for the collimator deliver a dose of 2 mm or smaller.

The positional accuracy experiment was preformed using a collimator prototype primarily manufactured from fused deposition modeling (FDM) 3D printing with a resolution of approximately 0.127 mm. The printing resolution limited the accuracy of the spur gears resulting in improper gear interference. The implementation of FDM spur gears in the collimator contributes to backlash in the mechanism. The backlash can be reduced if

the gears were manufactured from metal alloy and were held to a finer resolution, which would improve the gear interference. In addition, split gear can be implemented to reduce the backlash by offsetting half the gear to improve contact between gears (Figure 25). The backlash can be decreased by controlling the input of the collimator to increment to a desired leaf position from one direction. For an example, if the collimator were to use a clockwise input to increment to each leaf position, a counterclockwise input may be used to overshoot the desired position followed by the final clockwise input to increment to the desired leaf position. The same incrementing method was performed in the accuracy experiments to decrease the backlash of the collimator. In the experiment, the distance between leaves were measured to statistically determine the overall positional accuracy of the collimator; the experiment did not investigate the parallelism of the leaves.

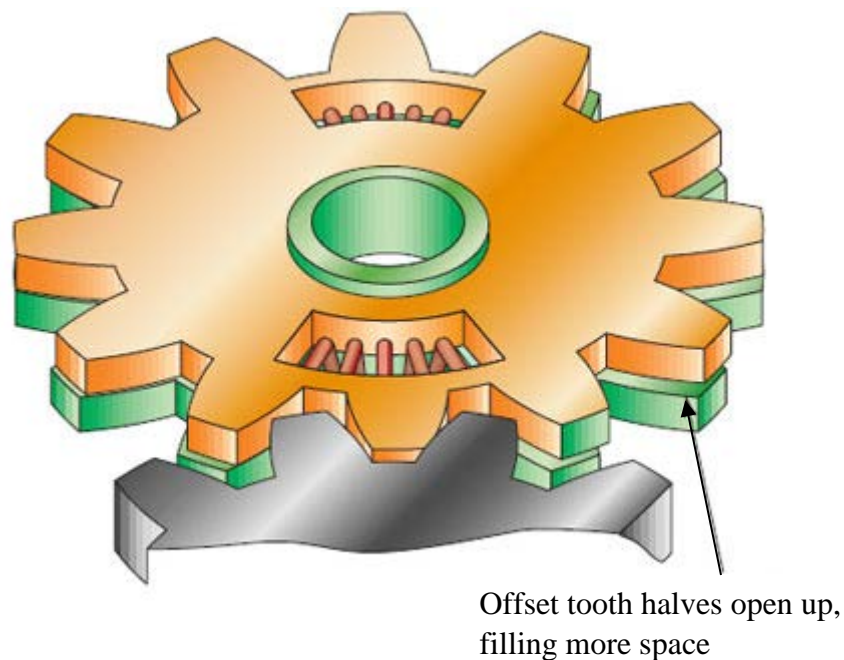


Figure 25: Split gear used to reduce backlash in gears

6.2 Discussion Dosimetry

In the dosimetry experiment, a Pantak DXT-300 unit was used to simulate an x-ray source. It should be noted that the focal spot size of the Pantak DXT-300 unit was 7 mm, resulting in a highly magnified diaphragm penumbra value of 1.9 mm. A focal spot size of the x-ray source being investigate for the SBIORT system has a focal spot size of approximately 2 mm. The geometrical relationship between the focal spot size of the radiation source and the penumbra value are shown in Figure 26 and in Equation 19, where f is the focal spot size, Pn is the penumbra value, H_1 , and H_2 are distances from the x-ray source to the obstruction and the obstruction to the surface, respectively.

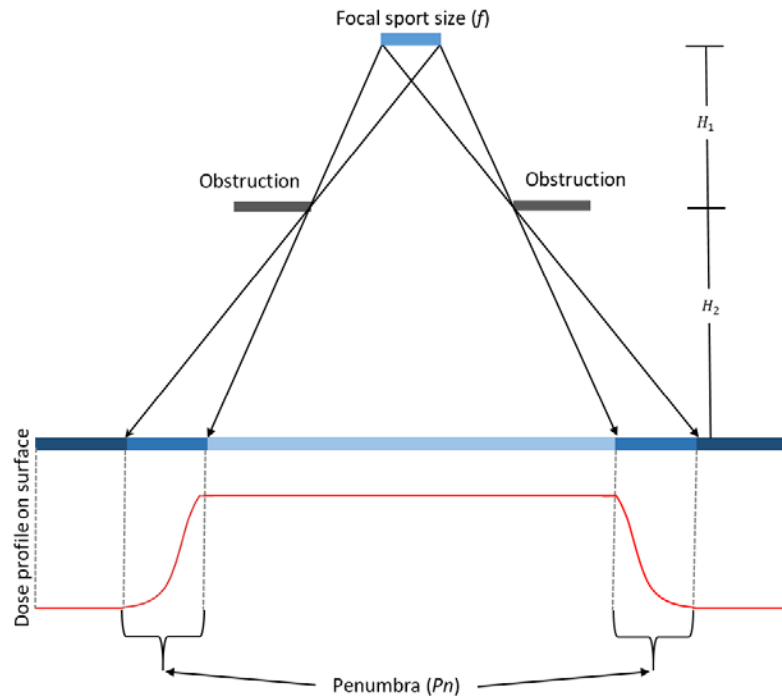


Figure 26: The geometrical relationship between the focal spot size of a radiation source and the penumbra size

$$Pn = f \left(\frac{H_2}{H_1} \right)$$

Equation 19

The FDM collimator prototype was used in the dosimetry experiment. The top of the collimator prototype was comprised of ABS plastic, approximately 2.8 mm thick; the delivered x-ray would pass through plastic cover and around the leaves of the collimator. To cover come the transmission of r-ray through the plastic cover, lead was positioned on the top of the collimator prototype to absorb the delivered x-ray. ABS plastic was used for prototyping the collimator, however the plastic would not be a suitable material for the SBIRT collimator; a material with a high attenuation coefficient would need to be used to absorb the delivered treatment.

Chapter 7 - Conclusion

Surgical resection has proven to be the preferred method of treatment for pancreatic cancer patients, resulting in a five-year survival rate in excess of 20%. Implementing IORT in the surgical procedure, reduces the regrowth of residual microscopic disease during post-operative convalescence time (weeks to months) required before EBRT can be administered. IORT reduces the treatment effects on healthy tissue that can be effected during EBRT. The development of the SBIORT system was motivated by the lack of imaging monitoring, portability, and collimation limitations of current IORT systems. A compact collimator was design for the SBIORT system for the delivery conformal radiation therapy.

Collimation systems used in EBRT and photography were investigated to determine the feasibility of implementation in the SBIORT system. MLC are widely used in conformal radiation therapy for EBRT systems. The MLC system provides highly conformal dose patterns with the use of individually positioned leaves. A compact MLC was designed for the SBIORT system. However, after altering a pre-existing MLC designs used in EBRT, it was determined that the footprint of the MLC design could not be effectively reduced for the design to be maneuvered in a surgical cavity. Optimization of the SBIORT MLC design resulted in a minimum cross section of 13 cm. An aperture design (similar to what is used in photograph) was investigated; the aperture design resulted in a collimation device that was compact is size (approximately 70 mm in diameter). The aperture design provided a variable square shaped field size controlled with a single radial input. Further analysis of the device's kinematic equations indicated angular deflection of the leaves as the device was cycled open and closed. Additional control of the device would

be required to correct the angular deflection of the leaves. The shortcomings of the MLC and aperture designs lead to the development of the current SBIORT collimation system.

The current SBIORT collimator design from four sets of four-bar linkages coupled together with the implementation of an internal spur gear, resulting in a collimation system with one degree of freedom. The SBIORT collimator can generate a variable square shaped aperture with the control of a single radial input. The compact diameter of collimator is approximately 66 mm and a height of 10 mm would allow the device to maneuver within the surgical cavity of a Whipple procedure. Utilizing a variable square shaped field size would enable for multiple doses to be aligned and conform to irregular tumor shapes. A maximum field size of 20 mm² would result is an estimated treatment time of approximately 40 min, a reasonable period for the implementation of IORT in a surgical procedure.

Prototypes of the SBIORT collimator were manufactured using fused deposition additive manufacturing. The leaves of the SBIORT collimator were machined from copper tungsten alloy. The collimator prototype was validated in positional accuracy experiments using image-processing techniques. The precision and bias errors from the positional accuracy experiment resulted in a total positional uncertainty of the collimator to be ± 0.25 mm, at a 95% confidence interval for a given input. The results of the SBIORT collimator positional accuracy results can be compare to the minimum tolerance of 0.5 mm for MLCs with widths of approximately 1 cm [24]. The positional accuracy of the SBIORT could be enhance by improving manufacturing processes and the material of internal components.

Dosimetry experiments were performed on the collimator prototype to determine the penumbra and transmission factor for the device. The transmission factor of the SBIORT collimator was measured to be 0.25%; this value can be compared to the larger MLC systems with transmission factors of 0.25-4% between leaves (depending on energy source) [24]. The penumbra of the SBIORT was measured to be 1.9 mm with a focal spot size of 7 mm. The focal spot size of the x-ray source used in the experiment was approximately 7 times larger than the focal spot size of smaller x-ray sources, which the SBIRT collimator is intended for. The ability to deliver doses was demonstrated in the dosimetry experiments, where the prototype SBIORT collimator was used to successfully generate a step dose distribution, using three separate doses.

The results from the positional accuracy and dosimetry experiments performed on the SBIORT collimator prototypes validate the device can be accurately deliver controlled radiation therapy. The compact size of the device would allow of maneuverability within the resectable pancreatic cancer surgical cavities. The SBIORT collimator proves to be a feasible option for delivering conformal radiation therapy in IORT.

References

- [1] A. Jemal, R. Siegel, E. Ward, T. Murray, J. Xu, and M. J. Thun, "Cancer statistics, 2007," (in eng), *CA Cancer J Clin*, vol. 57, no. 1, pp. 43-66, Jan-Feb 2007.
- [2] V. Valentini *et al.*, "Intra-operative radiotherapy (IORT) in pancreatic cancer: joint analysis of the ISORT-Europe experience," *Radiother Oncol*, vol. 91, no. 1, pp. 54-9, Apr 2009.
- [3] D. Li, K. Xie, R. Wolff, and J. L. Abbruzzese, "Pancreatic cancer," *Lancet*, vol. 363, no. 9414, pp. 1049-57, Mar 27 2004.
- [4] C. J. Yeo *et al.*, "Pancreaticoduodenectomy for cancer of the head of the pancreas. 201 patients," *Annals of surgery*, vol. 221, no. 6, p. 721, 1995.
- [5] N. Alexakis, C. Halloran, M. Raraty, P. Ghaneh, R. Sutton, and J. P. Neoptolemos, "Current standards of surgery for pancreatic cancer," *Br J Surg*, vol. 91, no. 11, pp. 1410-27, Nov 2004.
- [6] H. G. Beger, B. Rau, F. Gansauge, B. Poch, and K.-H. Link, "Treatment of pancreatic cancer: challenge of the facts," *World journal of surgery*, vol. 27, no. 10, pp. 1075-1084, 2003.
- [7] B. W. Kuvshinoff and M. P. Bryer, "Treatment of resectable and locally advanced pancreatic cancer," *Cancer Control*, vol. 7, no. 5, pp. 428-436, 2000.
- [8] T. A. Sohn *et al.*, "Resected adenocarcinoma of the pancreas-616 patients: results, outcomes, and prognostic indicators," (in eng), *J Gastrointest Surg*, vol. 4, no. 6, pp. 567-79, Nov-Dec 2000.
- [9] M. H. Kalser and S. S. Ellenberg, "Pancreatic cancer. Adjuvant combined radiation and chemotherapy following curative resection," (in eng), *Arch Surg*, Clinical Trial vol. 120, no. 8, pp. 899-903, Aug 1985.
- [10] A. Zerbi *et al.*, "Intraoperative radiation therapy adjuvant to resection in the treatment of pancreatic cancer," *Cancer*, vol. 73, no. 12, pp. 2930-5, Jun 15 1994.
- [11] C. A. Staley *et al.*, "Preoperative chemoradiation, pancreaticoduodenectomy, and intraoperative radiation therapy for adenocarcinoma of the pancreatic head," *The American journal of surgery*, vol. 171, no. 1, pp. 118-125, 1996.
- [12] S. Russo, J. Butler, R. Ove, and A. W. Blackstock, "Locally advanced pancreatic cancer: a review," (in eng), *Semin Oncol*, Review vol. 34, no. 4, pp. 327-34, Aug 2007.
- [13] C. Comas and P. A., "Irradiation roentgen itraabdominale, après intervention chirurgicale dans un cas de cancer de l'uterus," in *Congres International d'Electrologie* Barcelona: Imprenta Francesca Badia, 1907, pp. 5-14.
- [14] T. J. Kinsella and W. F. Sindelar, "Intraoperative radiotherapy for pancreatic carcinoma. Experimental and clinical studies," *Cancer*, vol. 78, no. 3 Suppl, pp. 598-604, Aug 1 1996.

- [15] M. Palta, C. Willett, and B. Czito, "The role of intraoperative radiation therapy in patients with pancreatic cancer," *Semin Radiat Oncol*, vol. 24, no. 2, pp. 126-31, Apr 2014.
- [16] G. A. Zygiogianni *et al.*, "Intraoperative radiation therapy on pancreatic cancer patients: a review of the literature," *Minerva Chir*, vol. 66, no. 4, pp. 361-9, Aug 2011.
- [17] C. G. Willett, B. G. Czito, and D. S. Tyler, "Intraoperative radiation therapy," *Journal of clinical oncology*, vol. 25, no. 8, pp. 971-977, 2007.
- [18] W. F. Sindelar, T. Kinsella, J. Tepper, E. L. Travis, S. A. Rosenberg, and E. Glatstein, "Experimental and clinical studies with intraoperative radiotherapy," *Surg Gynecol Obstet*, vol. 157, no. 3, pp. 205-19, Sep 1983.
- [19] J. B. Ashman *et al.*, "Preoperative chemoradiation and IOERT for unresectable or borderline resectable pancreas cancer," *J Gastrointest Oncol*, vol. 4, no. 4, pp. 352-60, Dec 2013.
- [20] R. Krempien and F. Roeder, "Intraoperative radiation therapy (IORT) in pancreatic cancer," *Radiation Oncology*, vol. 12, no. 1, p. 8, 2017.
- [21] Q. Liu, F. Schneider, L. Ma, F. Wenz, and C. Herskind, "Relative Biologic Effectiveness (RBE) of 50 kV X-rays measured in a phantom for intraoperative tumor-bed irradiation," *Int J Radiat Oncol Biol Phys*, vol. 85, no. 4, pp. 1127-33, Mar 15 2013.
- [22] D. J. Brenner, C. S. Leu, J. F. Beatty, and R. E. Shefer, "Clinical relative biological effectiveness of low-energy x-rays emitted by miniature x-ray devices," *Phys Med Biol*, vol. 44, no. 2, pp. 323-33, Feb 1999.
- [23] M. J. Zelefsky *et al.*, "High dose radiation delivered by intensity modulated conformal radiotherapy improves the outcome of localized prostate cancer," *The Journal of urology*, vol. 166, no. 3, pp. 876-881, 2001.
- [24] A. R. T. Committee and A. Boyer, *Basic applications of multileaf collimators*. American Association of Physicists in Medicine Madison, 2001.
- [25] D. Bullock, "Multi-Leaf Collimator", ed, 2007.
- [26] "Camera shutter mechanism," ed: Google Patents, 1961.
- [27] C. B. Bazzoni, "Photographic-camera shutter," ed: Google Patents, 1916.
- [28] M. E. Fox, "Camera shutter with oscillation damping," ed: Google Patents, 1994.
- [29] M. Heinze and W. Heinze, "Camera shutter," ed: Google Patents, 1978.
- [30] T.-C. Huang, "Camera shutter," ed: Google Patents, 2012.
- [31] S. C. Jones, "Photographic-camera shutter," ed: Google Patents, 1894.
- [32] K. Kanno, "Camera shutter system," ed: Google Patents, 1973.
- [33] G. F. Kincaid, "Photographic-camera shutter," ed: Google Patents, 1891.
- [34] K.-H. Lange, "High speed camera shutter," ed: Google Patents, 1976.
- [35] V. Nguyen, L. Switzer, and K. Takeuchi, "Camera shutter," ed: Google Patents, 2005.
- [36] L. Pbosch, "Camera-shutter," ed: Google Patents, 1891.
- [37] W. T. Rentschler, "Camera shutter with diaphragm and electro-magnetic drive for diaphragm," ed: Google Patents, 1977.
- [38] W. R. Savage, "Camera-shutter," ed: Google Patents, 1915.

- [39] G. Takeshi, "Camera shutter incorporating a governor mechanism," ed: Google Patents, 1972.
- [40] R. Tsai, "Mechanical camera shutter mechanism," ed: Google Patents, 2013.
- [41] A. Baab, "Iris diaphragm with linear aperture scale," ed: Google Patents, 1973.
- [42] S. Bamberger and A. Weiss, "Iris diaphragm device," ed: Google Patents, 2005.
- [43] P. J. Cade, L. H. Gallagher, and W. C. Sibley, "Iris diaphragm," ed: Google Patents, 1959.
- [44] B. Carl and B. Erich, "Iris diaphragm," ed: Google Patents, 1962.
- [45] J. Farnsworth, "Fully closing iris diaphragm," ed: Google Patents, 1974.
- [46] J. W. Graffley and R. J. Wollensak, "Iris diaphragm," ed: Google Patents, 1968.
- [47] T. Ide, "Iris diaphragm mechanism," ed: Google Patents, 2010.
- [48] F. Karl, "Iris diaphragm," ed: Google Patents, 1960.
- [49] M. E. Smith, "Iris-diaphragm," ed: Google Patents, 1915.
- [50] K. Woods, "Iris diaphragm," ed: Google Patents, 2005.
- [51] "Iris valve construction," ed: Google Patents, 1958.
- [52] A. Douglass, H. D. P. Aston, and W. Douglass, "Iris valve," ed: Google Patents, 1962.
- [53] W. P. Joachim, "Adjustable lock for iris valve," ed: Google Patents, 1960.
- [54] S. M. Werner, H. L. Davis, and M. R. Leach, "Iris valve for control of bulk solids," ed: Google Patents, 2006.
- [55] C. Wilcox, "Iris check valve and use thereof," ed: Google Patents, 1974.
- [56] D. Georg, F. Julia, E. Briot, D. Huyskens, U. Wolff, and A. Dutreix, "Dosimetric comparison of an integrated multileaf-collimator versus a conventional collimator," *Physics in medicine and biology*, vol. 42, no. 11, p. 2285, 1997.
- [57] C.-M. Ma *et al.*, "AAPM protocol for 40–300 kV x-ray beam dosimetry in radiotherapy and radiobiology," *Medical physics*, vol. 28, no. 6, pp. 868-893, 2001.